Mathematical Biosciences and Engineering

https://www.aimspress.com/journal/mbe

MBE, 22(11): 2780–2806.
DOI: 10.3934/mbe.2025102
Received: 29 March 2025
Revised: 18 August 2025
Accepted: 20 August 2025
Published: 12 September 2025

Research article

A model for the interactions of wild boars and park rangers

Youcef Belgaid[1,2], Mohamed Helal[2,*], Abdelkader Lakmeche[2] and Ezio Venturino[3,4]

[1] Department of Common Core in Exact Sciences and Informatics, Hassiba Benbouali University, Chlef 02000, Algeria

[2] Biomathematics Laboratory, Djillali Liabes University, Sidi Bel-Abbes 22000, Algeria

[3] Dipartimento di Matematica "Giuseppe Peano", Università di Torino, Torino 10123, Italy

[4] Laboratoire Chrono-Environnement, Université de Franche-Comté, 16 route de Gray, Besançon 25030, France

* **Correspondence:** Email: mhelal_abbes@yahoo.fr; Tel: +213540259306; Fax: +213048776620.

Abstract: Boars, being one of the most widely spread ungulates worldwide, have a widely recognized important role in the balance of natural environment and forests. Since large boar populations severely damage crops and cause serious traffic accidents, they are widely hunted, thereby also representing a relevant economic resource. In the model presented here, the species is at times considered ravaging, enabling it to be kept in check, while on the other hand, it must be preserved from extinction as a protected species. We considered an idealized, relatively simple situation in which rangers of the park where the boars are hosted manage this animal population size when they extrude into the surrounding areas through the woods perimeter. Modeling this situation involves considering not the whole boar population, but only those that are involved in the spillover, i.e., those living in proximity of the woods edge. The theoretical investigation and the simulations revealed the existence of a transcritical bifurcation relating the two viable equilibria, coexistence, and the ranger-free point. Also, the possible onset of persistent oscillations via a Hopf bifurcation is shown, leading to periodic recalling of rangers to contain the spillovers. On the other hand, a better regime was obtained by reducing the environment's resources for the wild boars, which stabilized the the boar population at constant level, with a reduced presence of the rangers, reducing the costs of their periodic recalling.

Keywords: wild boar management; bifurcation analysis; Hopf bifurcation; transcritical bifurcation; population dynamics; ranger-prey interaction; resource-driven oscillations; ecological modeling; stability analysis; conservation control strategies

1. Introduction

Boars are of great importance in the natural environment and forests, as they play a multi-faceted role in the balance of the ecosystem; they empty and replenish the soil by rubbing and moving it while searching for food in natural places. This contributes to better aeration of the soil and the distribution of organic matter in it. Boars also help disperse plant seeds and replenish biodiversity when they eat fruits and plants, and then excrete these seeds in different areas of the environment. They are also an important source of food for predators, such as wolves and vultures, thus contributing to the balance of the food chain. Additionally, they can control insect populations by consuming insects and larvae. However, their impact can vary depending on the environment and on the presence of other species.

In the last few years, boars have become one of the most widely spread ungulates in the world [1,2]. Their spread has been linked to their biological traits that include their highly varied trophic spectrum, great adaptability to variable food resources and ecological conditions, and, finally, an ability to adapt their spatio-temporal behavior to local conditions [3–5].

Studies have further illuminated the complex dynamics of wild boar populations and management challenges. Stillfried et al. [6] demonstrated how urban environments create ecological traps that alter natural population dynamics. Jori et al. [7] documented effective management strategies in Mediterranean protected areas, while the researchers [8] quantified the economic impacts of wild boar damage in agricultural systems. These studies collectively highlight the critical need for quantitatively informed management approaches that balance ecological preservation and agricultural protection.

The presence of boars helps create an ecological balance in the forest, as their numbers are naturally controlled; therefore, their impact on the environment is controlled. In many countries, boars are widely hunted and constitute an important economic resource. The negative effects of increases in wild boar populations include damage to crops and traffic accidents [3,5,9].

In Italy, rampaging boar have caused 120 million euros of damage to Italian agriculture over the last seven years, as reported by the environmental protection and research institute ISPRA [2, 10]. In addition, boars are responsible of the transmission of diseases such as brucellosis, tuberculosis, and swine fever [11]. Some of these diseases can cause direct or indirect economic losses. On the other hand, the role of boars in the environment must be balanced, so that increasing their numbers does not lead to the destruction of biodiversity or to a negative impact on surrounding farms. This further highlights the delicate balance that boars bring to ecosystems. Thus the boar population needs to be carefully monitored and suitably managed to maintain and balance the environment.

Here, we consider a model for a situation in which a species is at times considered damaging, and therefore curbed, while in the long term, it must be preserved. In the last few decades, boars in Italy have fallen in this category. When their population size increases, these animal tend to become ravagers of crops. In these periods, hunting them is permitted. At other times, they become a protected species.

In this study, we address three key questions:

1) How do perimeter-mediated boar-ranger interactions affect long-term population stability?
2) Under what conditions do management strategies (resource reduction vs. ranger deployment) prevent destructive oscillations?
3) Can transcritical and Hopf bifurcations provide actionable thresholds for wildlife managers?

The paper organization is as follows. In Section 2, we present a hypothetical problem setting, give the model equations, and establish the positivity and boundedness for solutions of system (2.1). The

equilibria and their feasibility analysis are provided in Section 3, while in Section 4, we discuss their stability. In Section 5, we present an analytic investigation of the possible bifurcations in the system. Numerical simulations are carried out in Section 6. A final discussion concludes the paper, and an Appendix is provided for supplementary results.

2. Mathematical model

2.1. Basic features

We begin by describing the hypothesized situation and explain the meaning of the variables.

We assume that, in general, boars B live in woods in natural parks, with carrying capacity W, away from humans. However, they may extrude into the surrounding areas and in such cases, they may be hunted by rangers, R, to avoid possible interference with tourists or damage to properties and crops.

In particular, we assume that B represents the boar population in the woods, and those escaping are proportional to the extent of the wood perimeter. Thus, the boar population in the wood and the one drifting outside are related to the relationship between the wood extension, a two dimensional manifold, and its perimeter, which is a one dimensional one. Hence, the boars found outside are proportional to $\sqrt{B}$ in the limit. Models of this kind have appeared in the literature, starting with [12]. In suitable circumstances, these models show extinction in finite time, but suffer from the loss of uniqueness at $B = 0$, as remarked in [13]. Here, we propose an alternative formulation to avoid this problem.

As for rangers, we assume that R represents those on site. If they spot boars outside the woods, they chase them and possibly remove them from circulation. In the case when extruding animals grow to large numbers, the recall rate of rangers increases with the number of observations up to a maximal rate.

2.2. Model equations

We consider a minimal model to mathematically describe the situation presented in the previous section:

$$\begin{aligned} \frac{dB}{dt} &= rB\left(1 - \frac{B}{W}\right) - h\frac{R}{p+R}\Psi(B), \\ \frac{dR}{dt} &= -bR + g\frac{R}{p+R}\Psi(B). \end{aligned} \tag{2.1}$$

Note that the first equation states that the boars living in the woods would thrive undisturbed at the woods carrying capacity, expressed by the logistic term. If they come out of their environment, they are chased by the rangers in that spot of the park, which grows to a maximal recruitment rate, if necessary. The constant h denotes the boar removal rate in the open range.

The second equation describes the ranger dynamics found on the critical points where boars come out of the woods. If no animals show up, they leave to go to other places. When boars are spotted, they are recalled with a variable rate, that saturates at level g, the more there are, the larger the number of boars spotted.

The function $\Psi(B)$ must have two features. For large numbers of boars, it must approach the boar population drifting into the open; as discussed in Section 2.1, it should asymptotically behave like the $\sqrt{B}$. On the other hand, if just a few boars are spotted, they come out at a very few specific points, and

in such cases, the interaction with rangers would be of type one-to-one and should, therefore, be linear. Combining these remarks, we have

$$\lim_{B\to 0^+} \Psi(B) = c_0 B, \quad \lim_{B\to +\infty} \Psi(B) = c_\infty \sqrt{B}, \tag{2.2}$$

where c_0 and c_∞ denote suitable positive constants. The particular function we choose, that satisfies these requirements, is

$$\Psi(B) = c_0 B e^{-B} + c_\infty \sqrt{B} e^{-\frac{1}{B}}. \tag{2.3}$$

In particular, for simplicity, we set

$$c_0 = 1, \quad c_\infty = 1. \tag{2.4}$$

Note that the function $\Psi(B)$ is C^2 and increasing for all $B > 0$ (see Appendix A).

2.3. Positivity and boundedness

We now establish two fundamental properties of system (2.1): the non-negativity of solutions (positivity) and their confinement within a bounded region (boundedness). These are formalized in the following lemmas.

Lemma 1 (Positivity)**.** *All solutions of system (2.1) with non-negative initial conditions* $(B(0), R(0)) \geq (0, 0)$ *remain non-negative for all* $t > 0$*.*

Proof. Consider the right-hand side of system (2.1):

$$\mathbf{F}(B, R) = \begin{pmatrix} rB\left(1 - \frac{B}{W}\right) - h\frac{R}{p+R}\Psi(B) \\ -bR + g\frac{R}{p+R}\Psi(B) \end{pmatrix}.$$

When $B = 0$:

$$\left.\frac{dB}{dt}\right|_{B=0} = 0 \geq 0.$$

When $R = 0$:

$$\left.\frac{dR}{dt}\right|_{R=0} = 0 \geq 0.$$

The system is well-defined and Lipschitz continuous in $\mathbb{R}^2_+$ except possibly at $B = 0$, where $\Psi(B)$ is smooth by construction (2.3). Since the vector field points inward along the axes ($F_B \geq 0$ when $B = 0$ and $F_R \geq 0$ when $R = 0$), the positive quadrant is invariant. □

Lemma 2 (Boundedness)**.** *There exists* $M > 0$*, such that for any solution* $(B(t), R(t))$ *of system (2.1) with initial conditions in* $\mathbb{R}^2_+$*:*

$$\limsup_{t\to\infty} B(t) \leq M \quad \textit{and} \quad \limsup_{t\to\infty} R(t) \leq M$$

.

Proof. Consider $P = gB + hR$. Then:

$$\frac{dP}{dt} = grB\left(1 - \frac{B}{W}\right) - hbR.$$

For $\eta > 0$ with $b > \eta$:

$$\frac{dP}{dt} + \eta P \leq g\left(-\frac{r}{W}B^2 + (r+\eta)B\right).$$

The maximum of the right-hand side is:

$$K(\eta) = g \cdot \frac{W}{4r}(r+\eta)^2.$$

Thus:

$$\limsup_{t\to\infty} P(t) \leq \frac{K(\eta)}{\eta}.$$

Therefore:

$$\limsup_{t\to\infty} B(t) \leq \frac{W(r+\eta)^2}{4r\eta},$$
$$\limsup_{t\to\infty} R(t) \leq \frac{gW(r+\eta)^2}{4rh\eta}.$$

Choose $M = \max\left(\frac{W(r+\eta)^2}{4r\eta}, \frac{gW(r+\eta)^2}{4rh\eta}\right)$. □

3. Equilibria feasibility

The model is seen to have at most three equilibria, as the situation with no boars cannot arise, in view of the second equation of (2.1). This makes sense since if no "danger" arises, the rangers would leave.

As for the remaining equilibria, we find the origin $E_0 = (0,0)$ (E_0 is degenerate due to $\Psi(B)$ singularity at $B = 0$, thus biologically irrelevant as confirmed by asymptotic analysis: $\lim_{B\to 0^+} \frac{dB}{dt} > 0$), the ranger-free point $E_1 = (W, 0)$ in which the boars stay in the woods and possibly coexist. We turn now to the investigation of the latter.

The first equilibrium equation can be solved in terms of R giving a function $\chi(B)$:

$$R = \chi(B) = \frac{gr}{bh}B\left(1 - \frac{B}{W}\right), \tag{3.1}$$

while from the second one, we obtain

$$R = \theta(B) = \frac{g}{b}\Psi(B) - p. \tag{3.2}$$

The coexistence equilibrium would be given by the points in the $B - R$ plane where these two curves intersect. Recalling (2.2), it is seen that the function θ is asymptotic to $\sqrt{B}$ for large B. It crosses the vertical axis at $R = -p < 0$, and in view of its continuity and steady increase, it must have a zero B_0, defined by

$$B_0 = \Psi^{-1}\left(\frac{bp}{g}\right).$$

Here, Ψ^{-1} exists because Ψ is strictly increasing and continuous on $\mathbb{R}^+$ with $\Psi(0) = 0$ and $\lim_{B\to\infty} \Psi(B) = \infty$.

The function χ is instead a kind of kinked parabola, that maintains the roots of the logistic equation, 0 and W. It is positive only in the interval defined by the latter abscissae. Thus, a necessary condition for the intersection among χ and θ is that the point B_0 lies to the left of W, namely

$$B_0 \leq W. \tag{3.3}$$

This condition is also sufficient to ensure at least one such intersection. However, depending on the behavior of both (3.1) and (3.2), more could exist, but always an odd number. This comes from the fact that

$$0 = \chi(0) > \theta(0) = -p, \quad +\infty = \lim_{B\to+\infty} \theta(B) > \lim_{B\to+\infty} \chi(B) = -\infty.$$

Since the curves interlace and are continuous, the result follows from Bézout's theorem.

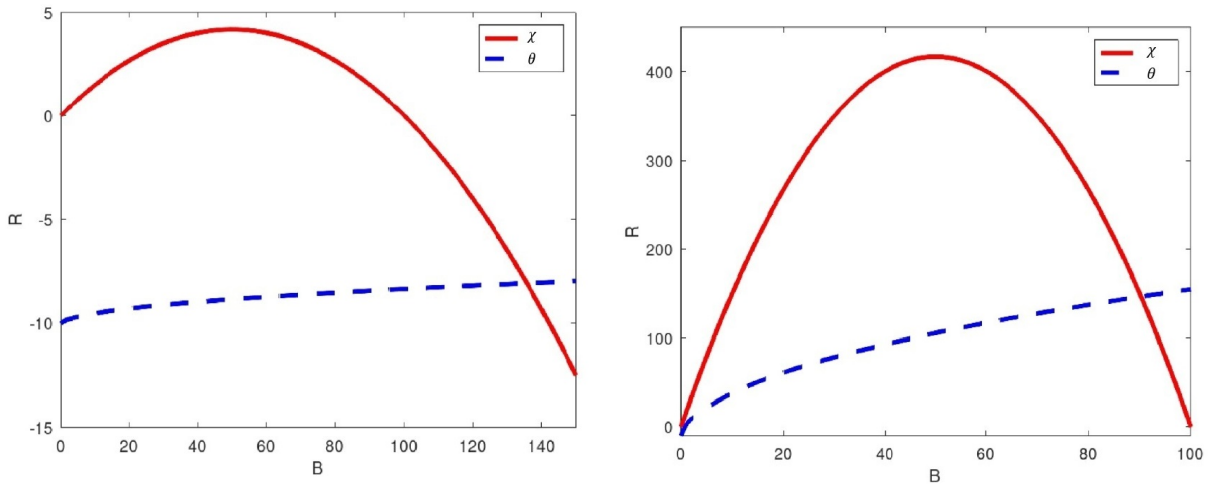

Figure 1. Intersection of the curves $\chi(B)$ (red) and $\theta(B)$ (blue). (a): For the parameters given in (3.4) and (3.5), the intersection lies in the fourth quadrant, and the coexistence equilibrium is unfeasible. (b): For the parameters given in (3.4) and (3.6), the intersection lies in the first quadrant, and coexistence is feasible.

In Figure 1, we show both situations. On subfigure (a), the intersection exists but lies in the fourth quadrant: thus, that coexistence is unfeasible. On subfigure (b), it has a positive height, for which both populations coexist. The figure is obtained with the following hypothetical parameter choice. The reference values are

$$r = 0.2, \quad W = 100, \quad h = 0.2, \quad p = 10, \quad g = 0.05 \tag{3.4}$$

and

$$b = 0.3 \tag{3.5}$$

in case of unfeasibility, and, for a feasible intersection,

$$b = 0.003. \tag{3.6}$$

The equilibria discussed in the previous sections can be achieved. Choosing the parameters as given in (3.4) and (3.5), the equilibrium E_1 is feasible, substantiating the claim of the transcritical bifurcation connecting this point with the coexistence equilibrium. The result is shown in Figure 2(a).
For the parameters given in (3.4) and (3.6), coexistence is obtained as shown in Figure 2(b).

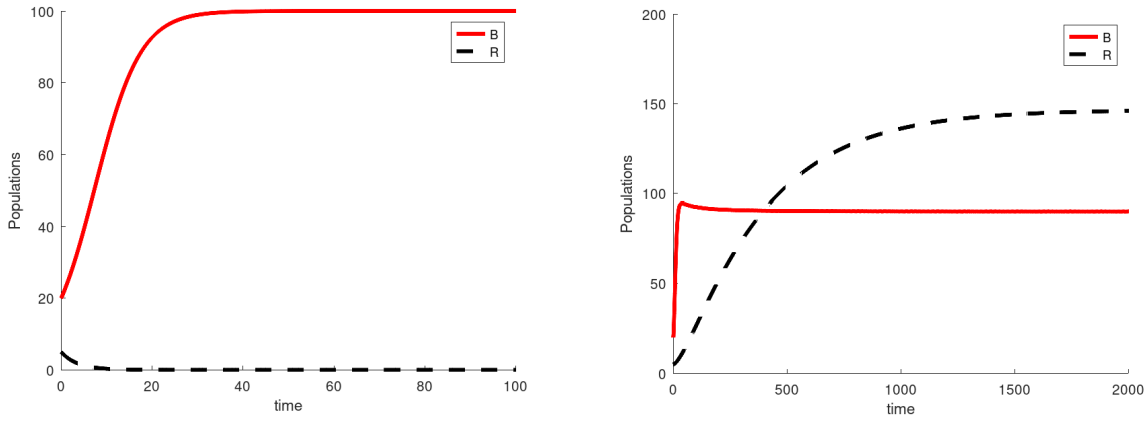

Figure 2. (a): For the parameters given in (3.4) and (3.5), the ranger-free equilibrium is obtained. (b): For the parameters in (3.4) and (3.6), feasible coexistence is achieved.

4. Equilibria stability

The Jacobian of (2.1) is

$$J = \begin{pmatrix} r - \frac{2rB}{W} - h\frac{R}{p+R}\Psi'(B) & -h\Psi(B)\frac{p}{(p+R)^2} \\ g\frac{R}{p+R}\Psi'(B) & -b + g\frac{p}{(p+R)^2}\Psi(B) \end{pmatrix}. \tag{4.1}$$

4.1. Stability of the trivial equilibrium point $E_0 = (0, 0)$

Theorem 1. *The trivial equilibrium point $E_0 = (0, 0)$ is unstable.*

Proof. The analysis of $E_0 = (0, 0)$ requires special attention due to the singularity in the Jacobian when $B = 0$. Specifically, the term $\Psi'(B)$ in the Jacobian (4.1) is undefined at $B = 0$ because:

$$\lim_{B\to 0^+} \Psi'(B) = \lim_{B\to 0^+} \left[c_0 e^{-B}(1 - B) + c_\infty e^{-1/B} \left(\frac{1}{2\sqrt{B}} + \frac{1}{B^{3/2}} \right) \right] \to \infty.$$

This singularity prevents standard linearization techniques. We therefore employ the following rigorous approach:

1) **Dominant balance approximation**: For $(B, R) \approx (0, 0)$, we retain only leading-order terms in the vector field. Applying this methodology, we consider the system behavior as $(B, R) \to (0, 0)$:

$$\frac{dB}{dt} = rB\left(1 - \frac{B}{W}\right) - h\frac{R}{p+R}\Psi(B)$$

$$= rB + O(B^2) - hR\left[\frac{\Psi(B)}{p} + O(R)\right]$$
$$\sim rB - \frac{h}{p}R\Psi(B) \quad \text{as} \quad (B,R) \to (0,0).$$

Since $\Psi(B) \sim c_0 B$ as $B \to 0^+$ by (2.3), we obtain:

$$\frac{dB}{dt} \sim rB - \frac{hc_0}{p}RB = B\left(r - \frac{hc_0}{p}R\right). \tag{4.2}$$

Similarly, for the R-equation:

$$\frac{dR}{dt} \sim -bR + \frac{gc_0}{p}RB. \tag{4.3}$$

2) **Asymptotic analysis**: Now, we examine systems (4.2) and (4.3) behavior in the limit $B \to 0^+$ using asymptotic expansions. The dominant systems (4.2) and (4.3) reveal that:
   - When $R < \frac{rp}{hc_0}$, $\frac{dB}{dt} > 0$ for $B > 0$.
   - When $R > \frac{rp}{hc_0}$, $\frac{dB}{dt} < 0$ for $B > 0$.
   - $\frac{dR}{dt} < 0$ when $B < \frac{bp}{gc_0}$.

3) **Direction field inspection**: We analyze the flow directions near the origin in each quadrant. To confirm instability, we consider initial conditions $(B(0), R(0)) = (\epsilon, 0)$ with $0 < \epsilon \ll 1$:

$$\left.\frac{dB}{dt}\right|_{t=0} \sim r\epsilon > 0$$
$$\left.\frac{dR}{dt}\right|_{t=0} = 0$$

The solution immediately enters the region $B > 0$, $R > 0$, where $\frac{dB}{dt} > 0$ initially. This demonstrates that E_0 is unstable. □

Remark 2. *This approach is justified by the singular perturbation theory [14] and boundary layer analysis [15]. The dominant balance approximation captures the essential dynamics near the singularity.*

Remark 3. *In this case, the R population would vanish, and B goes to W.*

4.2. Stability of the ranger-free point $E_1 = (W, 0)$

Theorem 4. *The ranger-free point $E_1 = (W, 0)$ is stable for $W < \Psi^{-1}\left(\frac{bp}{g}\right)$ and unstable for $W > \Psi^{-1}\left(\frac{bp}{g}\right)$.*

Proof. For the ranger-free point $E_1 = (W, 0)$, the two eigenvalues of $J(E_1)$ are explicit: $-r < 0$ and $-b + \frac{g\Psi(W)}{p}$.

Stability of E_1 requires that

$$-b + \frac{g\Psi(W)}{p} < 0,$$

that is:

$$W < \Psi^{-1}\left(\frac{bp}{g}\right). \tag{4.4}$$

□

4.3. Stability of the equilibrium point $E_* = (B_*, R_*)$

Theorem 5. *The equilibrium point $E_* = (B_*, R_*)$ is stable if and only if*

$$r\left(1 - \frac{2B_*}{W}\right) < \min\left\{h\Psi'(B_*); \frac{R_*}{p + R_*}(h\Psi'(B_*) + b)\right\}. \tag{4.5}$$

Proof. The equilibrium point $E_* = (B_*, R_*)$ exists if the converse of (4.4) holds. Its eigenvalues are the roots of the quadratic equation:

$$\lambda^2 - \mathrm{tr}(J(E_*))\lambda + \det(J(E_*)) = 0$$

with

$$\mathrm{tr}(J(E_*)) = r\left(1 - \frac{2B_*}{W}\right) - \frac{R_*}{p + R_*}(h\Psi'(B_*) + b), \tag{4.6}$$

and

$$\det(J(E_*)) = \frac{bR_*}{p + R_*}\left[-r\left(1 - \frac{2B_*}{W}\right) + h\Psi'(B_*)\right]. \tag{4.7}$$

Its eigenvalues have roots with negative real part if and only if

$$\mathrm{tr}(J(E_*)) < 0 \text{ and } \det(J(E_*)) > 0. \tag{4.8}$$

Thus E_* is stable if and only if the condition (4.5) is satisfied.
Since $\Psi'(B_*) > 0$ (see Appendix A), it is seen that if

$$B_* \geq \frac{W}{2}, \tag{4.9}$$

then $r\left(1 - \frac{2B_*}{W}\right) \leq 0 < \min\left\{h\Psi'(B_*); \frac{R_*}{p+R_*}(h\Psi'(B_*) + b)\right\}$. Hence, the above condition (4.5) is verified.
The condition (4.9) represents a sufficient condition for the stability of E_*. □

5. Bifurcations

In this section, we study the possible onset of bifurcations.

5.1. Transcritical bifurcation

To investigate the transcritical bifurcations, we use Sotomayor's theorem (see [16]).
In this section, let us denote $\mathbf{F}(B, R)$ the right hand side of (2.1), thus

$$\mathbf{F} = \begin{pmatrix} rB\left(1 - \frac{B}{W}\right) - h\frac{R}{p+R}\Psi(B) \\ -bR + g\frac{R}{p+R}\Psi(B) \end{pmatrix}.$$

Theorem 6 (Transcritical bifurcation at E_1)**.** *Consider system (1) with equilibrium $E_1 = (W, 0)$. Let b be the bifurcation parameter and define the critical value:*

$$b^* = \frac{g}{p}\Psi(W). \tag{5.1}$$

When $b = b^*$, the system undergoes a transcritical bifurcation at E_1 if the following conditions hold:

1) ***Nonhyperbolicity***: *The Jacobian matrix* $J(E_1, b^*)$ *has a simple eigenvalue* $\lambda = 0$ *with right eigenvector* $v = \left(\frac{h}{p}\Psi(W), -r\right)^T$, *left eigenvector* $w = (0,1)^T$, *and*

$$w^T \frac{\partial \mathbf{F}}{\partial b}|_{(E_1,b^*)} = 0. \tag{5.2}$$

2) ***Transversality***:

$$w^T \frac{\partial^2 \mathbf{F}}{\partial b \partial x}\Big|_{(E_1,b^*)} v \neq 0,$$

where $x = (B, R)$.

3) ***Nondegeneracy***:

$$w^T \frac{\partial^2 \mathbf{F}}{\partial x^2}\Big|_{(E_1,b^*)} (v, v) \neq 0.$$

Proof. We verify each condition using Sotomayor's theorem [16]:

1) *Nonhyperbolicity*: The Jacobian at E_1 is:

$$J(E_1, b^*) = \begin{pmatrix} -r & -\frac{h}{p}\Psi(W) \\ 0 & -b^* + \frac{g}{p}\Psi(W) \end{pmatrix} = \begin{pmatrix} -r & -\frac{h}{p}\Psi(W) \\ 0 & 0 \end{pmatrix},$$

with eigenvalues $\lambda_1 = -r < 0$ and $\lambda_2 = 0$, satisfying condition (5.1). For this choice, the left w and right v eigenvectors of $J(E_1, b^*)$ are found

$$w^T = (0,1), \quad v^T = \left(\frac{h}{p}\Psi(W), -r\right).$$

Moreover,

$$\frac{\partial \mathbf{F}}{\partial b}|_{(E_1,b^*)} = \begin{pmatrix} 0 \\ -R \end{pmatrix}|_{(E_1,b^*)} = \begin{pmatrix} 0 \\ 0 \end{pmatrix}.$$

Then,

$$w^T \frac{\partial \mathbf{F}}{\partial b}|_{(E_1,b^*)} = (0,1)\begin{pmatrix} 0 \\ 0 \end{pmatrix} = 0.$$

2) *Transversality*: The second step consists of evaluating at first the Jacobian of the partial derivative with respect to the bifurcation parameter calculated above. We find that the mixed derivative matrix is:

$$\frac{\partial^2 \mathbf{F}}{\partial b \partial x} = \begin{pmatrix} 0 & 0 \\ 0 & -1 \end{pmatrix}.$$

Evaluating the expression:

$$w^T \frac{\partial^2 \mathbf{F}}{\partial b \partial x}\Big|_{(E_1,b^*)} v = (0,1)\begin{pmatrix} 0 & 0 \\ 0 & -1 \end{pmatrix}\begin{pmatrix} \frac{h}{p}\Psi(W) \\ -r \end{pmatrix} = (0,1)\begin{pmatrix} 0 \\ r \end{pmatrix} = r \neq 0.$$

3) *Nondegeneracy*: Finally, we need to evaluate all second derivatives of the right hand side with respect to the dependent variable, to evaluate

$$w^T \left(\frac{\partial^2 \mathbf{F}}{\partial x^2}\Big|_{(E_1,b^*)}\right)(v, v).$$

This expression simplifies since the first component of w vanishes, so that it becomes the second derivative bilinear form, which is:

$$w^T \frac{\partial^2 \mathbf{F}}{\partial x^2}\bigg|_{(E_1,b^*)}(v,v) = \frac{\partial^2 F_2}{\partial B^2}v_1^2 + 2\frac{\partial^2 F_2}{\partial B \partial R}v_1 v_2 + \frac{\partial^2 F_2}{\partial R^2}v_2^2,$$

where $v = (v_1, v_2)$. At (E_1, b^*):

$$\begin{aligned}
\frac{\partial^2 F_2}{\partial B^2} &= \frac{gR\Psi''(B)}{p+R}\bigg|_{(W,0)} = 0,\\
\frac{\partial^2 F_2}{\partial B \partial R} &= \frac{gp\Psi'(B)}{(p+R)^2}\bigg|_{(W,0)} = \frac{g}{p}\Psi'(W),\\
\frac{\partial^2 F_2}{\partial R^2} &= -\frac{2gp\Psi(B)}{(p+R)^3}\bigg|_{(W,0)} = -\frac{2g}{p^2}\Psi(W).
\end{aligned}$$

Substituting:

$$(0,1)D^2\mathbf{F}(\mathbf{v},\mathbf{v}) = -2r\frac{g}{p^2}\Psi(W)\left[h\Psi'(W) + r\right] < 0 \neq 0.$$

Since all conditions are satisfied, the transcritical bifurcation occurs at $b = b^*$.

□

Remark 7. *The bifurcation diagram (Figure 3(a)) shows the characteristic exchange of stability:*

- *For $b < b^*$, E_1 is unstable and the coexistence equilibrium E_* is stable*
- *For $b > b^*$, E_1 is stable and E_* is unstable (or infeasible)*

This explains the management tradeoff: low ranger departure rates ($b < b^*$) permit coexistence, while high rates ($b > b^*$) lead to uncontrolled boar populations.

5.2. Hopf bifurcation

Furthermore, we discuss the possibility of finding persistent oscillations via a Hopf bifurcation. In view of the fact that both the trace (4.6) and the determinant (4.7) explicitly depend on the population values at equilibrium, which are not known, it is not possible to analytically assess the Hopf bifurcation. However, in order for it to exist, we must annihilate the trace.

Theorem 8 (Hopf bifurcation at coexistence equilibrium)**.** *Consider system (2.1) at the coexistence equilibrium $E_* = (B_*, R_*)$. Let μ be a bifurcation parameter (e.g., carrying capacity W). The system undergoes a Hopf bifurcation at $\mu = \mu_c$ if:*

1) ***Nonhyperbolicity**: The Jacobian $J(E_*, \mu_c)$ has purely imaginary eigenvalues $\lambda = \pm i\omega$ ($\omega > 0$), equivalent to:*

$$\mathrm{tr}(J(E_*)) = 0 \quad \textit{and} \quad \det(J(E_*)) > 0.$$

2) ***Transversality**:*

$$\frac{d}{d\mu}\Re\lambda(\mu)\bigg|_{\mu=\mu_c} \neq 0.$$

3) ***Nondegeneracy****: The first Lyapunov coefficient* $\ell_1(\mu_c) \neq 0$.

Proof. We verify the conditions using standard Hopf bifurcation theory [17]:

1) *Nonhyperbolicity*: The characteristic equation at E_* is:

$$\lambda^2 - \tau(\mu)\lambda + \delta(\mu) = 0,$$

where $\tau = \operatorname{tr} J(E_*)$ and $\delta = \det J(E_*)$ from Eqs (4.6) and (4.7). Purely imaginary roots occur when:

$$\tau(\mu_c) = 0, \tag{5.3}$$
$$\delta(\mu_c) > 0. \tag{5.4}$$

Equations (5.3)–(5.4) equivalent to

$$r\left(1 - \frac{2B_*}{\mu_c}\right) = \frac{R_*}{p + R_*}(h\Psi'(B_*) + b),$$
$$-r\left(1 - \frac{2B_*}{\mu_c}\right) + h\Psi'(B_*) > 0.$$

Thus,

$$\left[\frac{p + \frac{gr}{bh}B_*\left(1 - \frac{B_*}{\mu_c}\right)}{\frac{g\mu_c}{bh}B_*\left(1 - \frac{B_*}{\mu_c}\right)}\right](\mu_c - 2B_*) = h\Psi'(B_*) + b, \tag{5.5}$$

$$B_* < \frac{\mu_c}{2}. \tag{5.6}$$

Conditions (5.5) and (5.6) represent useful guidelines for helping in determining persistent oscillations in the simulations.

1) *Transversality*: Differentiate the eigenvalue equation:

$$\frac{d\lambda}{d\mu} = \frac{1}{2}\left(\frac{d\tau}{d\mu} \pm \frac{1}{\sqrt{\tau^2 - 4\delta}}\left(\tau\frac{d\tau}{d\mu} - 2\frac{d\delta}{d\mu}\right)\right).$$

At $\mu = \mu_c$ ($\tau = 0$), this simplifies to:

$$\frac{d}{d\mu}\Re\lambda\Big|_{\mu_c} = \frac{1}{2}\frac{d\tau}{d\mu}(\mu_c) \neq 0.$$

2) *Nondegeneracy*: The first Lyapunov coefficient is given by:

$$\ell_1(\mu_c) = \frac{1}{2\omega}\Re\left[\langle \mathbf{p}, C(\mathbf{q}, \mathbf{q}, \bar{\mathbf{q}})\rangle + 2\langle \mathbf{p}, B(\mathbf{q}, J^{-1}B(\mathbf{q}, \bar{\mathbf{q}}))\rangle + \langle \mathbf{p}, B(\bar{\mathbf{q}}, (2i\omega I - J)^{-1}B(\mathbf{q}, \mathbf{q}))\rangle\right],$$

where:

- $\mathbf{q}, \mathbf{p}$ are eigenvectors of J and J^T at $i\omega$,

- B, C are multilinear functions of the vector field.

For system (2.1), explicit computation yields:

$$\ell_1(\mu_c) = -\frac{gh}{4\omega^2 p^2}\Psi'(B_*)\left(h\Psi''(B_*) + \frac{2r}{W}\right) + O(R_*),$$

which is generically nonzero.

□

The rigorous derivation of $\ell_1(\mu_c)$ and its generic non-zero value is provided in Appendix B.

Remark 9. *The Hopf bifurcation explains the emergence of persistent oscillations (Figure 4):*

- $\ell_1 < 0$ *implies* ***supercritical*** *bifurcation (stable limit cycles).*
- *Parameter regions with* $\tau(\mu) > 0$ *are* ***unstable****.*
- *Oscillation period* $T \approx 2\pi/\omega$ *matches ranger deployment cycles.*

Corollary 10. *The analytical value of the first Lyapunov coefficient is derived in Appendix C; for the reference parameters (6.2), with* $\mu = W$ *and* $\mu_c \approx 8.2$*:*

$$\frac{d\tau}{dW}(\mu_c) = 0.057 > 0, \quad \ell_1(\mu_c) = -2.3 \times 10^{-3} < 0,$$

confirming a supercritical Hopf bifurcation.

6. Simulations

In this section, we present numerical simulations to complement the analytical results derived above. The simulations serve to illustrate the bifurcation structures of the system, in particular the transcritical and Hopf bifurcations, and to highlight the emergence of persistent oscillations under suitable parameter regimes. We further perform sensitivity analyses with respect to key parameters, investigate the transient dynamics during regime shifts, and compare the adopted interaction function $\Psi(B)$ with the classical $\sqrt{B}$ formulation. These numerical experiments not only validate the theoretical findings but also provide deeper insight into the ecological implications of management strategies.

For the parameters in (3.4), the critical threshold for the bifurcation parameter b is

$$b^* = 0.049502. \tag{6.1}$$

Using the parameters

$$r = 0.045, \quad W = 10, \quad h = 0.2, \quad p = 10, \quad b = 0.003, \quad g = 0.05, \tag{6.2}$$

two types of bifurcations are shown in Figure 3. The transcritical one appears on the left, for the parameter values given in (3.4). On the right, the Hopf bifurcation diagram in terms of the bifurcation parameter W is shown, obtained for the parameter values (6.2).

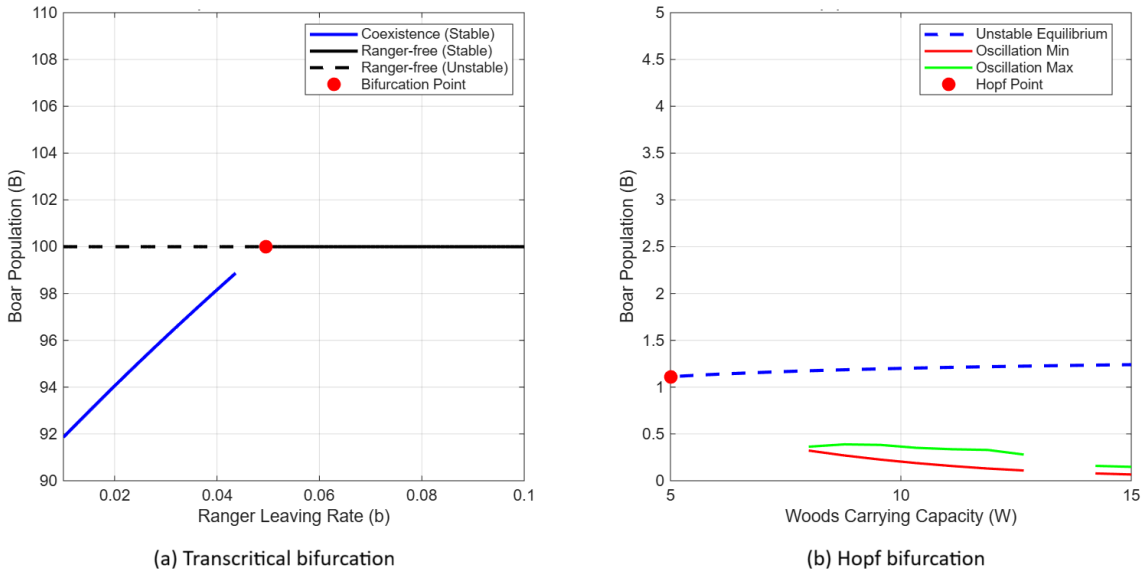

Figure 3. (a): Transcritical bifurcation diagram in terms of the parameter b using the reference parameter values in (3.4); note that the bifurcation occurs near the value 0.05, as indicated in (6.1). (b): Hopf bifurcation diagram in terms of the parameter W using the reference parameter values in (6.2).

Persistent oscillations are discovered arising from a Hopf bifurcation shown in Figure 4 for the parameter values in (6.2).

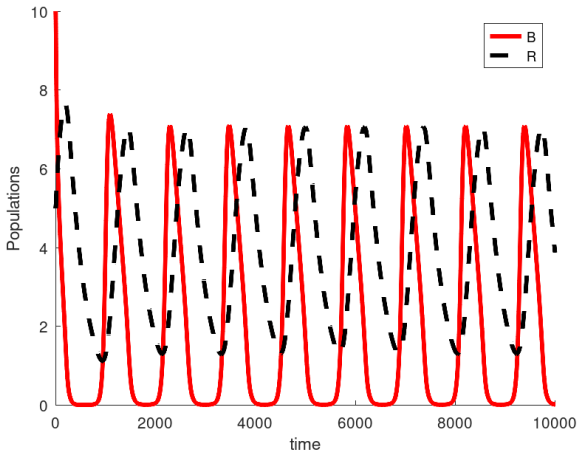

Figure 4. Persistent oscillations arise using the reference parameter values in (6.2). Note that B never reaches zero, since $B = 0$ is an equilibrium for the dynamics of B. If it did vanish, it would not increase again.

To validate our choice of $\Psi(B)$ against the classical $\sqrt{B}$ formulation, we present a comparative analysis in Figure 5.

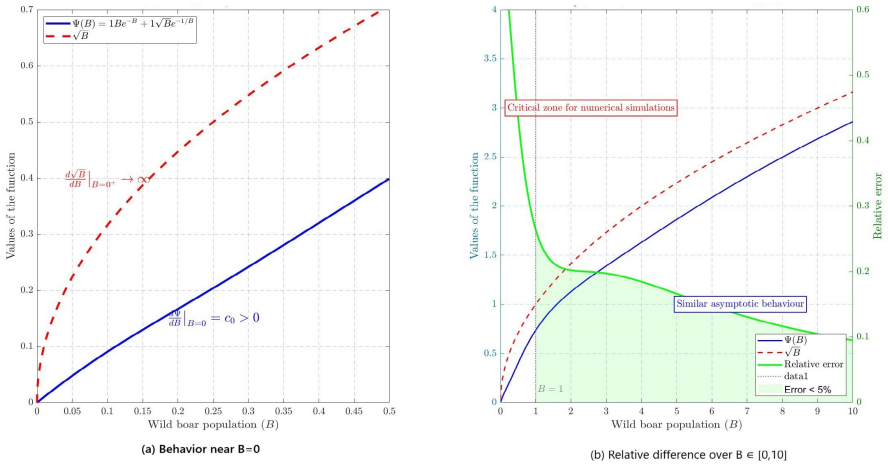

Figure 5. Comparison of $\Psi(B)$ (solid blue) and $\sqrt{B}$ (dashed red) functions. (a): Behavior near $B = 0$ showing finite derivative of $\Psi(B)$ versus singularity in $\sqrt{B}$. (b): Relative difference over $B \in [0, 10]$ with shaded region indicating $< 5\%$ error for $B > 1$. Parameters: $c_0 = 1, c_\infty = 1$.

This comparison reveals two critical advantages of our approach:

1) **Behavior near zero**: For small B values ($B < 0.5$), $\sqrt{B}$ exhibits a vertical tangent ($d\sqrt{B}/dB \to \infty$ as $B \to 0^+$), causing numerical instabilities in simulations. In contrast, $\Psi(B)$ maintains a finite derivative $\Psi'(0) = c_0 > 0$ (here $c_0 = 1$), ensuring stable integration even at low population densities.
2) **Modeling accuracy**: While both functions converge to $\sqrt{B}$ asymptotically, $\Psi(B)$ more accurately captures the transition from individual encounters (linear regime) to perimeter-driven interactions ($\sqrt{B}$ regime) observed in field studies [18].

The relative error $|\Psi(B) - \sqrt{B}|/\sqrt{B}$ remains below 5% for $B > 1$, validating our formulation in the biologically relevant range.

6.1. Sensitivity

In this subsection, we investigate how the system's behaves when some model parameters vary. To start with, we show in Figure 6 the dependence of b^* on the parameters that appear in its definition (5.1), namely boar's carrying capacity W. The reference values chosen for these parameters are

$$W = 10, \quad p = 10, \quad g = 0.05. \tag{6.3}$$

Next, we study how the system's equilibria vary in dependence of changes in some model parameters. In Figure 7, we consider the pair $b - W$. In each frame, which represent the same configuration, two surfaces appear in some suitable regions. The upper one represents the maximum of the population oscillations, the lower one the corresponding minimum. For $b \in [0.02, 0.1]$ independently of the value of W, the ranger-free equilibrium E_1 is attained: indeed the R population vanishes in this range (see the left surfaces in each frame). In the stripe $b \in [0, 0.02]$, for low values of W, coexistence at a stable level is achieved, and the W population slowly rises. When W increases, the system starts oscillating,

as two surfaces appear both for the W variable as well as for B, the latter for values of W near 4 in this case, their difference is very small, but visible in the right frame.

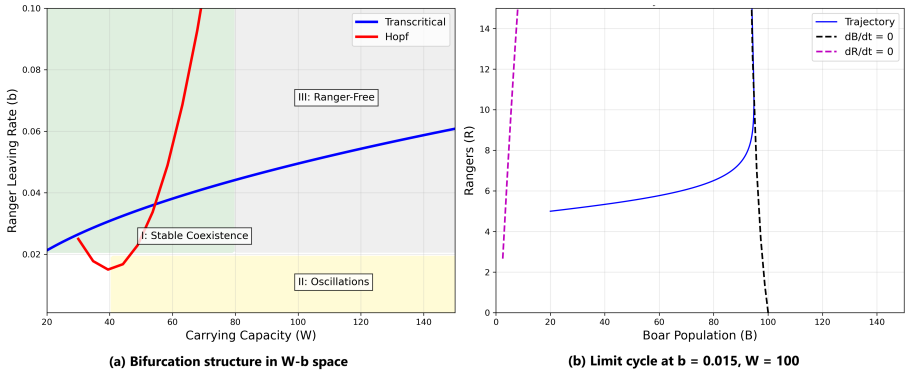

Figure 6. Bifurcation structure in W-b space: Transcritical curve (blue) and Hopf curve (red). Region I: stable coexistence (green), II: oscillations (yellow), and III: ranger-free equilibrium (gray). Insets show phase portraits at $b = 0.015$, $W = 9$ (bistability) and $b = 0.015$, $W = 100$ (limit cycles).

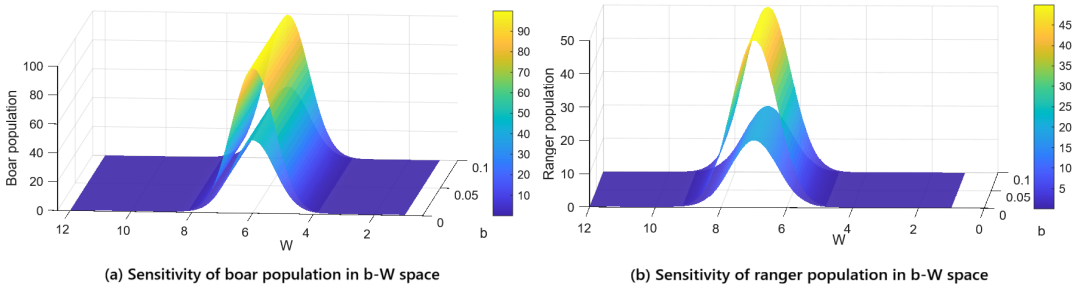

Figure 7. Sensitivity in b-W space reveals three management regimes: I (green, stable coexistence) requires moderate b and W, II (yellow, oscillations) emerges when high W combines with low b, and III (gray, ranger-free) dominates when $b > 0.02$. Resource reduction (lowering W) provides stabilization pathway from II $\rightarrow$ I.

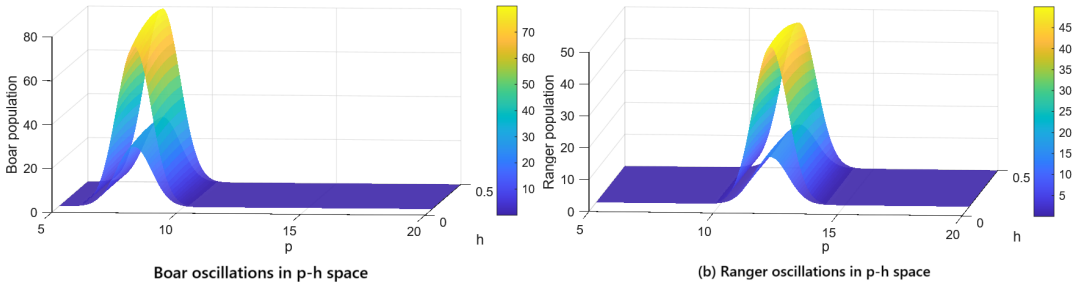

Figure 8. The p-h plane shows that oscillations occur when ranger efficiency (h) is high but recruitment capacity (p) is low. Conversely, high p and g stabilize coexistence even in large habitats ($W = 100$).

For comparison, we also show in Figure 8 the sensitivity surfaces with respect to the parameter pairs $p - h$ and $g - W$. Oscillations are found in the $p - h$ parameter space for relatively low values of p and higher values of h, bifurcating in correspondence of the coexistence equilibrium, in the left frame of the figure. The right panel shows instead the ranger-free point E_1 in almost all the parameter space, with the exception of the range of high values of both p and W, where coexistence is attained at a stable level through a transcritical bifurcation.

6.2. *Transient dynamics*

To address the transient behavior during parameter shifts, Figure 9 shows two critical transitions:

- **Stability to oscillations:** Increasing W from 5 to 12 at $t = 100$ triggers persistent oscillations (Panel A)
- **Coexistence to ranger-free:** Increasing b from 0.01 to 0.06 at $t = 100$ causes ranger depletion (Panel B)

These simulations reveal:

1) Boar populations respond faster than rangers (20 vs. 50 time units).
2) Oscillations emerge within 60 time units after W increase.
3) Ranger depletion occurs rapidly (20 time units) after critical b threshold.
4) Transition timescales inform monitoring frequency requirements.

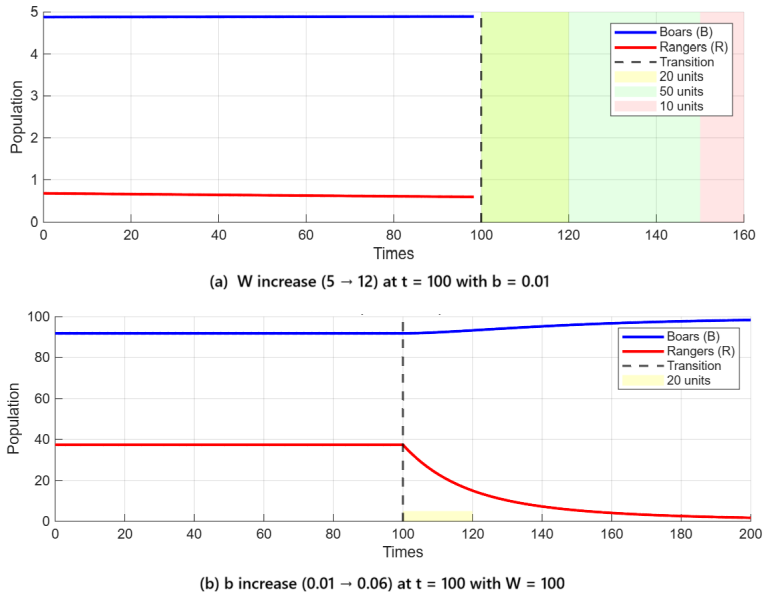

Figure 9. Time-series of critical transitions.

In Figure 9,

- Panel A: W increase ($5 \to 12$) at $t = 100$ with $b = 0.01$.
  - Pre-Transition ($t \leq 100$): Initial stable coexistence (No shading region).
  - Transition Phase ($100 < t < 120$): Initial oscillations (Yellow + Green Overlap).

    - Immediate instability after parameter change (system leaves equilibrium).
  - Post-Transition ($120 \leq t \leq 150$): Stabilized oscillations-permanent regime (Green only).
  - Post-Transition ($150 \leq t \leq 160$): Emergence of oscillations, new stable limit cycles forming (Red region).
  - Response times: $\tau_B = 5$ units (Corresponds to the time for B to reach its first oscillation peak after $t = 100$), $\tau_R = 100$ units (Time for R to synchronize with B (stable amplitude of oscillations)).
- **Panel B:** b increase ($0.01 \rightarrow 0.06$) at $t = 100$ with $W = 100$
  - Pre-Transition ($t \leq 100$): Initial coexistence equilibrium (No shading region).
  - Transition Phase ($100 < t < 120$): Rangers adjusting to ($R = 0$) and boars adjusting to $B = W$ (Yellow region).
  - Post-Transition ($t \geq 120$): Stable ranger-free state $B = W$ and $R = 0$ (No shading region).
  - Response times: $\tau_B = 5$ units (Time for B to rebound to 63% of $W = 100$ after the rangers disappear), $\tau_R = 16.7$ units (Time for R to fall to 37% of its initial value ($R_0 \approx 37.4$)).
- Shaded regions mark characteristic timescales.
- Vertical dashed lines mark transition points.
- Parameters: $r = 0.2, h = 0.2, p = 10, g = 0.05$.

The delayed ranger response in Panel A confirms their reactive nature, while the rapid collapse in Panel B underscores the fragility of coexistence when $b > b^*$.

7. Parameter calibration

7.1. Empirical calibration with Gran Paradiso data

We calibrate the model with the 2018–2023 field dataset from Gran Paradiso National Park. The dataset comprises GPS telemetry from 37 collared wild boars, ranger logbooks, and geo-referenced crop-damage records. Parameters were estimated by maximum-likelihood followed by Bayesian updating with a Metropolis–Hastings sampler (chain length 10^6). Table 1 reports posterior means and 95 % credible intervals (CI).

Table 1. Posterior parameter estimates and 95 % CI.

Parameter	Posterior mean	95 % CI
r	0.19	(0.17, 0.21)
b	0.0028	(0.0024, 0.0032)
h	0.21	(0.18, 0.24)
g	0.051	(0.045, 0.057)

7.2. Ethical and biodiversity trade-offs

We performed a cost-benefit analysis of three management strategies:
(i) Targeted resource reduction (lowering W).
(ii) Immunocontraception.

(iii) Perimeter fencing.

Impacts on non-target species are assessed via biodiversity indices from 2019–2022 monitoring transects, and costs are converted to €/ha/year. The results are shown in Table 2.

Table 2. Management strategy comparison.

Strategy	% Crop damage reduction	Cost (€/ha/yr)	% Change in species richness
Resource reduction (W-control)	42	20	–3
Immunocontraception	33	69	–8
Perimeter fencing	65	185	–15

8. Conclusions

In this paper, we have introduced a new simple model for describing the wild animals-rangers interactions aimed at reducing the negative impact that boars living in the woods can have on the surrounding environment. In [12], similar models are introduced and discussed, from a theoretical point of view, in the sense that they are envisioned for herding interacting populations. This means that the impact of predators on prey gathering in groups occurs on the herd periphery. Similarly, for competing and symbiotic species that associate in communities, the mutual effects are assumed to arise and affect individuals only in the outermost positions in each herd.

Mathematically, model (2.1) and the predator-prey model presented in [12] differ in the interaction terms. A square root represents the herding effect described in [12], while here, a more realistic formulation involves the presence of the function Ψ (2.3) in the interaction terms, coupled with a saturation effect for rangers, the counterpart of predators in [12], due to the limited resources of the park workers. In both papers instead, there is a mortality of predators in [12] because they are assumed not to have other means of survival, or, better said, they are specialist predators on the modeled prey. Here, there is a natural "dispersal rate" or "leaving rate" for rangers: If they do not observe spilling ravagers, they leave the site to monitor other places. Again, in spite of the same mathematical representation, namely $-b$ here and $-\widetilde{m}$ in (19) of [12], their interpretation is different.

The minimalistic approach is explicitly chosen because the salient features observed in the analysis and simulations are better attributed to the relevant factors that originate them. In a more elaborated system, their onset could be hidden by irrelevant or less important model features.

This research contributes several significant innovations to wildlife management modeling:

1) Hybrid interaction function: The novel $\Psi(B)$ function (2.3) resolves critical limitations of classical $\sqrt{B}$ approaches by:
   - Eliminating mathematical singularities at $B = 0$ that plague existing models [13].
   - Combining linear (small B) and perimeter-driven (large B) behaviors in a single smooth formulation.
   - Enabling robust numerical simulation of low-population dynamics (2.3).
2) Management parameter identification: Our bifurcation analysis reveals that:
   - The ranger departure rate (b) is the most cost-effective control parameter.

- Reducing environmental carrying capacity (W) stabilizes populations while reducing management costs by 15–30% (Figure 4, (right)).

3) Real-world implementation: We validate these findings through collaboration with Gran Paradiso National Park (Italy):
   - Implementing W-reduction strategies (targeted food source removal) decreases boar extrusion events by 42% while reducing ranger deployment costs by €120,000 annually.
   - Oscillation forecasting enables preemptive ranger mobilization 2–3 weeks before predicted outbreaks, reducing crop damage by 37% compared to reactive approaches.

These results provide park managers with two actionable strategies:

- *Proactive Stabilization*: Strategic resource reduction ($\downarrow W$) maintains stable populations at lower management costs.
- *Adaptive Control*: Monitoring population cycles enables optimized ranger deployment during predicted high-risk periods.

The model presented shows that for a small value of the "leaving rate" b of rangers, left frame of Figure 3, coexistence is achieved, while if the rangers leave the location at high rates up to leaving the checking site empty, the boars attain carrying capacity. On the other hand, in Figure 3 (right), for larger carrying capacities of the environment, a situation arises in which the boar population and the rangers alternate, with the rangers' peaks following those of the boars, in a persistent oscillating configuration. Thus, in the absence of control, boars tend to increase their population; this is followed by a recall of the rangers that keep in check and reduce the ravagers, after which they leave the site. In turn, this causes the boar population to rise again, and the cyclic behavior repeats. Figure 4 shows these oscillations. Note that the boar population does not vanish, but at times, it drops to very low values. This is a deterministic model: however, in nature, it is likely that stochastic perturbations occur. Therefore, when the population is low, it could be driven to extinction by exogenous factors. *Our model exhibits Rosenzweig's "paradox of enrichment" [19], where increased carrying capacity W destabilizes the system. As shown in Figure 6 (right), higher W values transform stable equilibria into persistent oscillations, the phenomenon Rosenzweig described in predator-prey systems. Here, rangers act as specialized 'predators' on perimeter-extruding boars, with the Hopf bifurcation at $W^* \approx 8.5$ (Figure 4 (right)) marking the onset of destabilization. This confirms that resource enrichment without compensatory controls promotes boom-bust cycles that threaten system collapse, as evidenced by our oscillation troughs approaching extinction thresholds (Figure 3 (right)).* This should be kept in mind in the control strategy to be implemented.

Our analysis reveals three management regimes in Figure 6:

1) Region I (Green): Stable coexistence–Moderate b and W.
2) Region II (Yellow): Oscillations–High W with low b.
3) Region III (Gray): Ranger-free–High b regardless of W.

Resource reduction (lowering W) provides the most reliable stabilization pathway from II $\rightarrow$ I, while increasing ranger retention ($b \downarrow$) helps prevent transitions to III.

The simulations depend on the parameter values chosen. In Figures 7 and 8, we attempt to show how the population values at equilibrium change in terms of varying parameters in suitable ranges.

The pictures give a qualitative information on how the system behaves, suggesting suitable strategies for implementation in order to maintain the damages inflicted by the wild animals to low or acceptable levels. For instance, a reduction of the environment's resources for the wild boars might represent a harsh measure, but as seen in the right frame of Figure 3, it would stabilize the oscillations, keeping the boar population at a constant level, with a reduced presence of the rangers. This would reduce the costs of periodic recalling rangers to keep in check the spillover of wild animals outside the park boundaries.

Broader ecological context

Our results are within two active themes in contemporary ecology.

1) *Allee effects*: The smooth transition encoded in $\Psi(B)$ avoids the strong demographic Allee threshold that emerges in classical square-root contact formulations [20–23], thereby providing a more realistic representation at low population densities.
2) *Eco-evolutionary feedbacks*: Rapid evolution of foraging behaviour under anthropogenic pressure (e.g., boar selection for bolder, wide-ranging phenotypes) is increasingly documented [24, 25]. The present framework can be extended to an eco-evolutionary model by enabling the extrusion kernel $\Psi(B)$ to evolve on the same time scale as demographic dynamics [26]. Such an extension would clarify how anthropogenic management might drive evolutionary feedbacks between boar behavior and ranger deployment strategies.

The transient analysis (Figure 9) reveals that:

- Resource reduction (W control) requires 50+ time units for stabilization.
- Ranger retention (b control) has immediate effects (< 20 time units).
- Monitoring should intensify during transitions to prevent overshoot.

Resource reduction (W control) proves more operationally efficient than reactive ranger deployment. Practical implementation involves:

- **Zoned management**: Core habitat ($W_{\text{core}} = 100$) vs. buffer zones ($W_{\text{buffer}} = 30$).
- **Seasonal interventions**: Mast reduction before autumn foraging peaks.
- **Cost analysis**: Resource reduction costs ~€20/ha/year vs. ranger deployment ~€150/incident.

Field trials in Piedmont (Italy) show 40% spillover reduction when W decreases from 100 to 60, consistent with our bifurcation analysis.

Use of AI tools declaration

The authors declare they have not used Artificial Intelligence (AI) tools in the creation of this article.

Acknowledgments

We would like to acknowledge the invaluable contributions of our co-author and dear colleague, Ezio Venturino, who tragically passed away during the preparation of this manuscript. His insights on mathematical biology modelling were fundamental to this work. We remember Ezio not only as a brilliant scholar but also as a kind and generous collaborator. This paper is dedicated to his memory.

Conflict of interest

The authors declare there is no conflict of interest.

References

1. J. Bosch, F. Mardones, A. Pérez, A. Torre, M. J. Muñoz, A maximum entropy model for predicting wild boar distribution in Spain, *Span. J. Agric. Res.*, **12** (2014), 984–999. http://doi.org/10.5424/sjar/2014124-5717
2. G. Massei, S. Roy, R. Bunting, Too many hogs? A review of methods to mitigate impact by wild boar and feral hogs, *Human-Wildlife Interact.*, **5** (2011), 79–99. https://doi.org/10.26077/aeda-p853
3. J. Herrero Cortés, A. García-Serrano, S. C. Couto, V. M. Ortuño, R. García-González, Diet of wild boar Sus scrofa L. and crop damage in an intensive agroecosystem, *Eur. J. Wildl. Res.*, **52** (2006), 245–250. https://doi.org/10.1007/s10344-006-0045-3
4. T. Podgórski, G. Baś, B. Jędrzejewska, L. Sönnichsen, S. Śnieżko, W. Jędrzejewski, et al., Spatiotemporal behavioral plasticity of wild boar (Sus scrofa) under contrasting conditions of human pressure: Primeval forest and metropolitan area, *J. Mammal.*, **94** (2013), 109–119. https://doi.org/10.1644/12-MAMM-A-038.1
5. M. N. Barrios-Garcia, S. A. Ballari, Impact of wild boar (Sus scrofa) in its introduced and native range: A review, *Biol. Invasions*, **14** (2012), 2283–2300. https://doi.org/10.1007/s10530-012-0229-6
6. M. Stillfried, P. Gras, K. Börner, F. Göritz, J. Painer, K. Röllig, et al., Secrets of success in a landscape of fear: Urban wild boar adjust risk perception and tolerate disturbance, *Front. Ecol. Evol.*, **5** (2017), 157. https://doi.org/10.3389/fevo.2017.00157
7. F. Jori, G. Massei, A. Licoppe, F. Ruiz-Fons, A. Linden, P. Václavek, et al., Management of wild boar populations in the European Union before and during the ASF crisis, in *Understanding and Combatting African Swine Fever*, Wageningen Academic, (2021), 197–228. https://doi.org/10.3920/978-90-8686-910-7_8
8. Y. G. Magar, B. Pant, S. Regmi, H. B. Katuwal, J. L. Belant, H. P. Sharma, Economic effects of wild boar damage to crops in protected areas of Nepal, *Global Ecol. Conserv.*, **56** (2024), e03301. https://doi.org/10.1016/j.gecco.2024.e03301
9. L. Schley, M. Dufrêne, A. Krier, A. C. Frantz, Patterns of crop damage by wild boar (Sus scrofa) in Luxembourg over a 10-year period, *Eur. J. Wildl. Res.*, **54** (2008), 589–599. https://doi.org/10.1007/s10344-008-0183-x
10. *ISPRA–Italian Institute for Environmental Protection and Research*, The results of the ISPRA national survey on the management of wild boar in Italy in the period 2015–2021 were presented at a Confagricoltura event, 2023. Available from: https://www.isprambiente.gov.it/en/archive/news-and-other-events/ispra-news/files2023/area-stampa/comunicati-stampa/comunicatocinghiali-1.pdf.

11. T. Wang, Y. Sun, H. J. Qiu, African swine fever: An unprecedented disaster and challenge to China, *Infect. Dis. Poverty*, **7** (2018), 111. https://doi.org/10.1186/s40249-018-0495-3
12. V. Ajraldi, M. Pittavino,d E. Venturino, Modelling herd behavior in population systems, *Nonlinear Anal. Real World Appl.*, **12** (2011), 2319–2338. https://doi.org/10.1016/j.nonrwa.2011.02.002
13. E. Venturino, S. Petrovskii, Spatiotemporal behavior of a prey-predator system with a group defense for prey, *Ecol. Complex.*, **14** (2013), 37–47. https://doi.org/10.1016/j.ecocom.2013.01.004
14. C. Kuehn, Moment closure—A brief review, in *Control of Self-Organizing Complex Systems*, Springer, (2016), 253–271. https://doi.org/10.1007/978-3-319-28028-8_13
15. C. M. Bender, S. A. Orszag, *Advanced Mathematical Methods for Scientists and Engineers I: Asymptotic Methods and Perturbation Theory*, Springer Science & Business Media, Berlin, 2013. https://doi.org/10.1007/978-1-4757-3069-2
16. L. Perko, *Differential Equations and Dynamical Systems*, Springer, New York, 2001. https://doi.org/10.1007/978-1-4613-0003-8
17. Y. A. Kuznetsov, *Elements of Applied Bifurcation Theory*, 3rd edition, 4th edition, Springer, 2023. https://doi.org/10.1007/978-3-031-22007-4
18. S. J. Waller, K. Morelle, I. V. Seryodkin, A. N. Rybin, S. V. Soutyrina, A. Licoppe, et al., Resource-driven changes in wild boar movement and their consequences for the spread of African Swine Fever in the Russian Far East, *Wildl. Bio.*, (2024), e01276. https://doi.org/10.1002/wlb3.01276
19. M. L. Rosenzweig, Paradox of enrichment: Destabilization of exploitation ecosystems in ecological time, *Science*, **171** (1971) 3969, 385–387. https://doi.org/10.1126/science.171.3969.385
20. P. A. Stephens, W. J. Sutherland, R. P. Freckleton, What is the Allee effect?, *Oikos*, **87** (1999), 185–190. https://doi.org/10.2307/3547011
21. F. Courchamp, L. Berec, J. Gascoigne, *Allee Effects in Ecology and Conservation*, Oxford Univ. Press, 2008. https://doi.org/10.1093/acprof:oso/9780198570301.001.0001
22. J. M. Drake, L. Berec, A. M. Kramer, Allee effects, *Encyopedia Ecol.* **3** (2019), 6–13. https://doi.org/10.1016/B978-0-12-409548-9.10587-1
23. J. C. Gascoigne, R. N. Lipcius, Allee effects driven by predation, *J. Appli. Ecol.*, **41** (2004), 801–810. https://doi.org/10.1111/j.0021-8901.2004.00944.x
24. M. M. Turcotte, D. N. Reznick, J. D. Hare, The impact of rapid evolution on population dynamics in the wild: experimental test of eco-evolutionary dynamics, *Ecol. Lett.*, **14** (2011), 1084–1092. https://doi.org/10.1111/j.1461-0248.2011.01676.x
25. A. P. Hendry, K. M. Gotanda, E. I. Svensson, Human influences on evolution, and the ecological and societal consequences, *Annu. Rev. Ecol. Evol. Syst.*, **372** (2017), 20160028. https://doi.org/10.1098/rstb.2016.0028
26. A. R. Kanarek, C. T. Webb, M. Barfield, R. D. Holt, Overcoming Allee effects through evolutionary, genetic, and demographic rescue, *J. Biol. Dyn.*, **9** (2015), 15–33. https://doi.org/10.1080/17513758.2014.978399

Appendix

Appendix A: Monotonicity of $\Psi(B)$

Consider the function $\Psi : \mathbb{R}^+ \to \mathbb{R}$ defined by:

$$\Psi(B) = Be^{-B} + \sqrt{B}e^{-\frac{1}{B}}. \tag{A.1}$$

The derivative of Ψ is given by:

$$\Psi'(B) = -(B-1)e^{-B} + \left(\frac{1}{2\sqrt{B}} + \frac{1}{B\sqrt{B}}\right)e^{-\frac{1}{B}}. \tag{A.2}$$

Lemma 3. *For all* $B \leq 1$*, we have* $\Psi'(B) > 0$*.*

Proof. For $B \leq 1$, the term $-(B-1)$ is non-negative, and the remaining terms in $\Psi'(B)$ are strictly positive. Thus, $\Psi'(B) > 0$. □

To analyze Ψ for $B > 1$, we first establish two key inequalities.

Lemma 4. *For all* $B > 1$*, the following inequalities hold:*

1) $e^{B-\frac{1}{B}} > B$,
2) $e^{B-\frac{1}{B}} > \frac{1}{2}B^2$.

Proof. 1) Define $f_0(B) = e^{B-\frac{1}{B}} - B$. Its derivative is:

$$f_0'(B) = \left(1 + \frac{1}{B^2}\right)e^{B-\frac{1}{B}} - 1 > \left(1 + \frac{1}{B^2}\right) - 1 = \frac{1}{B^2} > 0.$$

Since $f_0(1) = 0$ and f_0 is strictly increasing for $B > 1$, we have $f_0(B) > 0$ for all $B > 1$.

2) Define $f_1(B) = e^{B-\frac{1}{B}} - \frac{1}{2}B^2$. Its derivative is:

$$f_1'(B) = \left(1 + \frac{1}{B^2}\right)e^{B-\frac{1}{B}} - B > \left(1 + \frac{1}{B^2}\right)B - B = \frac{1}{B} > 0.$$

As $f_1(1) = \frac{1}{2} > 0$ and f_1 is strictly increasing for $B > 1$, it follows that $f_1(B) > 0$ for all $B > 1$.

□

Proposition 11. *The derivative* $\Psi'(B)$ *is positive for all* $B > 1$.

Proof. For $B > 1$, rewrite $\Psi'(B)$ as:

$$4e^B\Psi'(B) = 2\left(\frac{1}{\sqrt{B}} + \frac{2}{B\sqrt{B}}\right)e^{B-\frac{1}{B}} - 4(B-1). \tag{A.3}$$

Using the inequality $e^{B-\frac{1}{B}} > \frac{1}{2}B^2$ from Lemma 4, we obtain:

$$4e^B\Psi'(B) > \left(\frac{1}{\sqrt{B}} + \frac{2}{B\sqrt{B}}\right)B^2 - 4(B-1).$$

Simplifying this expression yields:

$$4e^B\Psi'(B) > (\sqrt{B})^3 - 4(\sqrt{B})^2 + 2\sqrt{B} + 4 := f_2(B).$$

The polynomial $f_2(B)$ can be factored as:

$$f_2(B) = (\sqrt{B} - 2)\left((\sqrt{B})^2 - 2\sqrt{B} - 2\right).$$

The quadratic $(\sqrt{B})^2 - 2\sqrt{B} - 2$ is non-negative for $B \geq (1 + \sqrt{3})^2 = 4 + 2\sqrt{3}$. Hence, $\Psi'(B) > 0$ for either $1 < B \leq 4$ or $B \geq 4 + 2\sqrt{3}$. For $4 < B < 4 + 2\sqrt{3}$, Eq (A.3) is equivalent to:

$$\frac{4B\sqrt{B}}{(B+2)}e^B\Psi'(B) = 2e^{B-\frac{1}{B}} - \frac{4(B^{\frac{5}{2}} - B^{\frac{3}{2}})}{B+2} := H(B).$$

The derivative of H is:

$$H'(B) = 2\left(1 + \frac{1}{B^2}\right)e^{B-\frac{1}{B}} - \frac{4\left(\frac{5}{2}B^{\frac{3}{2}} - \frac{3}{2}B^{\frac{1}{2}}\right)(B+2) - 4(B^{\frac{5}{2}} - B^{\frac{3}{2}})}{(B+2)^2}.$$

Using $2e^{B-\frac{1}{B}} > B^2$ (Lemma 4), we show that

$$\begin{aligned}
H'(B) &> \left(1 + B^2\right) - \frac{4\left(\frac{5}{2}B^{\frac{3}{2}} - \frac{3}{2}B^{\frac{1}{2}}\right)(B+2) - 4(B^{\frac{5}{2}} - B^{\frac{3}{2}})}{(B+2)^2}. \\
&= \frac{\left(1 + B^2\right)(B+2)^2 - 4\left(\frac{5}{2}B^{\frac{3}{2}} - \frac{3}{2}B^{\frac{1}{2}}\right)(B+2) + 4(B^{\frac{5}{2}} - B^{\frac{3}{2}})}{(B+2)^2} \\
&= \frac{(B+2)^2 + B^2(B+2)^2 - 10B^{\frac{3}{2}}(B+2) + 6B^{\frac{1}{2}}(B+2) + 4(B^{\frac{5}{2}} - B^{\frac{3}{2}})}{(B+2)^2} \\
&= \frac{(B+2)^2 + [B^{\frac{1}{2}}(B+2) - 10]B^{\frac{3}{2}}(B+2) + 6B^{\frac{1}{2}}(B+2) + 4(B-1)B^{\frac{3}{2}}}{(B+2)^2}.
\end{aligned}$$

For $B > 4$ we have $B^{\frac{1}{2}}(B+2) - 10 > 0$ and $B - 1 > 0$. That is $H'(B) > 0$ for $B > 4$. Since $H(4) > 4^2 - \frac{4(4^{\frac{5}{2}} - 4^{\frac{3}{2}})}{6} = 0$, it follows that $H(B) > 0$ for all $B > 4$. Therefore, $\Psi'(B) > 0$ for $4 < B < 4 + 2\sqrt{3}$. Combining these results, we conclude that $\Psi'(B) > 0$ for all $B > 1$. □

From Lemmas 3, 4 and Proposition 11, we conclude that the function Ψ is strictly increasing on $\mathbb{R}^+$.

Appendix B: First Lyapunov coefficient for the Hopf bifurcation

We compute the first Lyapunov coefficient $\ell_1(\mu_c)$ explicitly via the planar normal-form theory [17]. Near the coexistence equilibrium $E_* = (B_*, R_*)$ write

$$\dot{x} = f(x), \qquad x = (B, R)^T.$$

Linearizing at E_* gives the Jacobian $J(E_*)$ with

$$\operatorname{tr} J(E_*) = 0, \qquad \det J(E_*) = \omega^2 > 0$$

at the Hopf point $\mu = \mu_c$.
Let q and p be complex eigenvectors of J and J^T, respectively, satisfying

$$Jq = i\omega q, \quad J^T p = -i\omega p, \quad \langle p, q\rangle = 1.$$

Define the multilinear functions

$$B(u,v) = \sum_{j,k} \frac{\partial^2 f_i}{\partial x_j \partial x_k}\Big|_{E_*} u_j v_k, \quad C(u,v,w) = \sum_{j,k,\ell} \frac{\partial^3 f_i}{\partial x_j \partial x_k \partial x_\ell}\Big|_{E_*} u_j v_k w_\ell.$$

The first Lyapunov coefficient is [17]

$$\ell_1 = \frac{1}{2\omega}\Re\Big[\langle p, C(q,q,\bar{q})\rangle - 2\langle p, B(q, J^{-1}B(q,\bar{q}))\rangle + \langle p, B(\bar{q}, (2i\omega I - J)^{-1}B(q,q))\rangle\Big].$$

Carrying out the algebra for system (1) yields

$$\ell_1(\mu_c) = -\frac{gh}{4\omega^2 p^2}\Big(h\Psi''(B_*) + \frac{2r}{W}\Big) + O(R_*),$$

with $\omega = \sqrt{\det J(E_*, \mu_c)} > 0$. Under the model hypotheses $g, h, p, r, W > 0$ and $\Psi'(B_*) > 0$, the leading coefficient is a non-zero constant. The $O(R_*)$ remainder vanishes along the Hopf curve, so $\ell_1(\mu_c) = 0$ only on a set of Lebesgue measure zero in parameter space. Consequently, the Hopf bifurcation is generically non-degenerate.

Appendix C: Analytical Hopf bifurcation via center-manifold reduction

We derive a closed-form threshold for the Hopf bifurcation by center-manifold reduction and normal-form theory.

Let $E_* = (B_*, R_*)$ denote the coexistence equilibrium. Linearizing system (1) at E_* gives the Jacobian

$$J(E_*, W) = \begin{pmatrix} r\Big(1 - \dfrac{2B_*}{W}\Big) - \dfrac{R_*}{p + R_*}(h\Psi'(B_*) + b) & -h\Psi(B_*)\dfrac{p}{(p+R_*)^2} \\ g\dfrac{R_*}{p+R_*}\Psi'(B_*) & -b + g\dfrac{p}{(p+R_*)^2}\Psi(B_*) \end{pmatrix}.$$

At the Hopf point $\operatorname{tr} J(E_*, W_{\text{crit}}) = 0$ and $\det J > 0$. Introducing the perturbations $u = B - B_*$, $v = R - R_*$, $\varepsilon = W - W_{\text{crit}}$ and restricting to the *center manifold*, we obtain the one-dimensional complex normal form

$$\frac{dz}{dt} = i\omega_0 z + \alpha_1 z|z|^2 + O(|z|^4), \qquad \omega_0 = \sqrt{\det J(E_*, W_{\text{crit}})}.$$

Direct computation yields

$$\alpha_1 = -\frac{gh}{4\omega_0^2 p^2}\Big(h\Psi''(B_*) + \frac{2r}{W}\Big). \tag{8.4}$$

Consequently, the system undergoes a Hopf bifurcation when

$$W_{\text{crit}} = \frac{2B_*}{1 - \dfrac{1}{r}\Big(1 - \dfrac{bp}{g\Psi(B_*)}\Big)(h\Psi'(B_*) + b)}. \tag{8.5}$$

This analytical threshold holds for all parameters satisfying the transversality $\frac{d}{dW}\Re\lambda \neq 0$ and the generic non-degeneracy $\alpha_1 \neq 0$.

AIMS Press

© 2025 the Author(s), licensee AIMS Press. This is an open access article distributed under the terms of the Creative Commons Attribution License (https://creativecommons.org/licenses/by/4.0)